International Journal of Adhesion & Adhesives 64 (2016) 168–178

Contents lists available at ScienceDirect

International Journal of Adhesion & Adhesives

journal homepage: www.elsevier.com/locate/ijadhadh

Identification of kissing defects in adhesive bonds using infrared thermography

Rachael C. Tighe*, Janice M. Dulieu-Barton, Simon Quinn

Faculty of Engineering and the Environment, University of Southampton, Highfield, Southampton SO17 1BJ, United Kingdom

ARTICLE INFO

Article history:
Accepted 16 October 2015
Available online 28 October 2015

Keywords:
C. Non-destructive testing
C. Thermal analysis
B. Composites
Kissing defects
Pulse phase thermography

ABSTRACT

A carbon fibre reinforced plastic (CFRP) adhesively bonded single lap joint sample is used for comparing the detection of different defect types using pulsed phase thermography (PPT). Firstly, a polytetrafluoroethene (PTFE) insert, of the type widely used to simulate defects in composite materials, was added to the bond line of the joint. Liquid layer kissing defects were simulated using silicon grease. PPT clearly identified the PTFE but not the silicon grease contamination. The PPT identified the silicon grease defect when the joint was loaded. It is postulated that kissing defects can be detected using thermography if a small load is applied to the joint, as loading opens the defect and produces a gap that provides sufficient thermal contrast for detection. Thermoelastic stress analysis (TSA) is used to validate the approach. On-site application is addressed both in terms of the load application and the use of low cost infrared (IR) detectors.

1. Introduction

Sensitive and reliable non-destructive methods of detecting defects in adhesive bonds must be identified to enable adhesive bonds to be used in primary structural roles. Such non-destructive evaluation (NDE) approaches should be suitable for use in the field and provide efficient and rapid inspection over potentially large areas.

There are several types of defects that can occur in adhesive bonds. These defect types can be broadly split into three categories: voids, inclusions and low volume/kissing defects. Voids and inclusions are relatively easy to detect using a range of NDE techniques as they generally have different properties to the surrounding materials. A variation in material density greatly aids defect detection when using ultrasound, where as a variation in heat transfer properties enhances the thermal contrast for detection using thermographic approaches. The final, and most elusive, type of defect may be called a low volume defect or kissing defect [1].

A kissing defect can be defined as the improper adhesion of adhesive to adherend. Physically, kissing defects are low volume defects that have material properties that are similar to the surrounding materials and therefore do not provide sufficient contrast to be detected using typical NDE procedures. There are several theories [2] of the cause of kissing defects, including: contamination, improper adhesive curing or mixing and variations in environmental conditions during joint construction.

In the present investigation it was necessary to define a means of creating simulated kissing defects in known locations. It has been suggested that simulated kissing defects can be produced in two ways: dry contact and liquid layer [1]. The dry contact bond is achieved by compressively loading an adherend to precured adhesive to achieve intimate contact with zero adhesion across the entire bond. Dry contact defects have been investigated using ultrasonic techniques [3–5] where the nonlinearity of the response was found to be inversely related to the amount of compressive load, i.e. the degree of contact of the two surfaces. A liquid layer kissing defect is created by adding of a small amount of contaminant to the bond line, e.g. [6,7]. This type of simulated kissing defect is more realistic in terms of adhesive bonds as it can be introduced to just part of the bond with the surrounding area bonded. Ultrasonic detectability of liquid layer defects have also been investigated [1] using basic c-scans on a realistic bond and with compressive loading applied uniformly across the bond area. It was found above a low level (5 MPa) of compression that the reflection coefficient is reduced for the defect thus decreasing the likelihood of detection if any leakage path exists for the liquid layer to escape through. Where this liquid layer is contained the increase in pressure reduced the reflection coefficient more gradually. The literature shows that NDE of adhesive bonds is typically carried out using ultrasound. However, ultrasound is a generally a time consuming process often requiring coupling with the material to obtain the highest sensitivity.

There have been some applications of thermographic approaches to the identification of defects in bonded joints, e.g. [8,9] , however these have been based on identification of a region of

* Corresponding author.
E-mail address: rcw1n09@soton.ac.uk (R.C. Tighe).

http://dx.doi.org/10.1016/j.ijadhadh.2015.10.018
0143-7496/

distinct differing thermal properties, such as flat bottom holes, air gaps, full delamination and inserts. Kissing defects contain far less thermal contrast than has been created in these cases. Pulsed thermography (PT) data may be processed into pulse phase thermography (PPT) phase data to enhance the detectability of low contrast defects via use of a fast Fourier transform (FFT) [10].

While promising results have been obtained using ultrasonic approaches, the purpose of the present paper is to investigate an alternative method for identification of kissing defects based on thermography. Liquid layer defects in bonded joints are investigated and it is demonstrated that the defects can be classified as kissing defects. A comparison of the thermal response from a PTFE insert, representative of a typical composite calibration sample, and the simulated kissing defects is described. As PPT relies on thermal contrast between the defect and bulk material of the joint, the work investigates if the application a small load can help identify a kissing defect. A literature review has been conducted to ascertain if such a proposition has been explored previously. A US patent has been filed describing an idea [11] but no subsequent research or experimental proof of concept is in the public domain. For validation purposes thermoelastic stress analysis (TSA) [12] is used to analyse stress fields on the surface of the joints. A single lap joint configuration with simulated defects in the bond line is used so that TSA and PPT could be carried out whilst loading in a standard servo-hydraulic test machine. A finite element model establishes the minimum gap the loading must produce to provide sufficient thermal contrast for kissing defect identification. Finally, the feasibility of using a vacuum loading to open a kissing defect is investigated.

2. Experimental procedure

2.1. Thermographic techniques

2.1.1. Pulse phase thermography

PPT is an active thermographic method where a pulse of heat is applied to the surface of a component and the thermal evolution on the surface is monitored using an infrared (IR) detector [13,14]. The current work focusses on the use of PPT in the reflection mode shown in Fig. 1a with heat source and detector focussed on the same surface of the component [15]. Reflection mode requires only single sided access making it versatile and suited to a wide range of on-site applications. Heat is pulsed onto the surface of the component. The surface temperature decays as the heat front propagates through the thickness of the material. If the heat transfer properties below the surface are laterally uniform across the observed area, the surface temperature will decay uniformly. If there is a region of different thermal properties this will cause a change in the rate of heat transfer through that region and result in an area of different temperature on the surface directly over this region [16], as shown in Fig. 1b. This region of different thermal properties may be a defect within the material. Direct analysis of this thermal data is known as PT. In PPT the thermal data is processed using a FFT. Phase values are produced with reference to a generated sinusoidal wave. The frequency of the wave is selected to be appropriate to the material and geometry of the component being tested. A range of frequencies is typically used to inspect the full thickness of a sample, as in lock-in or modulated thermography [17]. The extraction of phase data typically enables deeper and more sensitive probing of the component as experimental variations such as uneven surface heating and optical surface features are removed [18].

2.1.2. Thermoelastic stress analysis

In TSA a component is usually subjected to a cyclic tensile load within the elastic region of the sample. An IR detector is used to monitor the surface of the component. The cyclic load induces a small temperature change due to the thermoelastic effect [19]. The temperature data collected may be related to the sum of the principal stresses, $\Delta(\sigma_1 + \sigma_2)$, using,

$$\Delta T = -\frac{\alpha T}{\rho C_p}\Delta(\sigma_1+\sigma_2) \quad (1)$$

where ΔT is the temperature change, T is the absolute temperature of the surface of the material, α is the coefficient of linear thermal expansion, ρ is the density and C_p is the specific heat. Eq. (1) is only valid where the temperature change occurs isentropically (i.e., no heat transfer, plasticity, dissipation etc.). It is also assumed that material properties are such that they are independent of temperature. The thermal data is processed using a lock-in amplification routine with the applied cyclic load used as a reference signal. Therefore the magnitude and phase of ΔT are obtained. The phase data contains information about the synchronisation of the loading and the thermal response.

2.2. Sample preparation

Single lap joints were manufactured from $[0, 90]_{2s}$ carbon fibre reinforced epoxy resin pre-preg SE84LV by Gurit. Pieces of the same CFRP panel were used as spacers to reduce the bending moment in the lap joint, as in Fig. 2. The bond was made using Araldite rapid curing epoxy adhesive with a total bond area of 30x30 mm^2 and a bond thickness of 0.2 mm. Defect material of 10x10 mm^2 was added to the bond line to create defect. Three defect materials were used: 0.02 mm thick polytetrafluoroethene (PTFE), Frekote mould release agent and silicon grease. Specimens without defects were used as control specimens to compare mechanical properties. The PTFE was a loose insert cut to size to be used as a thermal control sample to establish experimental parameters for PPT and TSA experiments. The silicon grease and

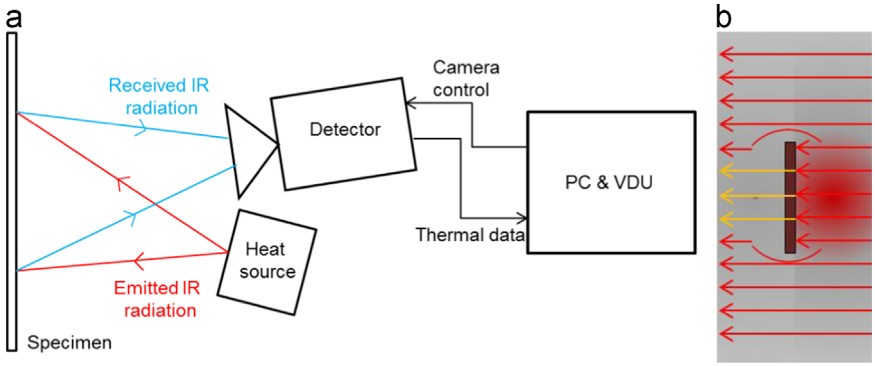

Fig. 1. Pulse phase thermography, showing (a) a schematic of the experimental setup and (b) variations in heat flow through defect and non-defect regions.

Frekote release agent aimed to simulate kissing defects by applying them to one of the adherends of the lap using a stencil. The silicon grease was applied in a single layer using a spatula and the Frekote was applied in six layers using a cloth to minimise bleeding. The adhesive was applied to the opposite adherend to minimise smearing of the contaminants. The bond was cured at room temperature with a pressure of 0.3 MPa applied uniformly across the joint for at least 3 hours, until the adhesive was fully cured. Testing was carried out at least 24 hours after joint manufacture. All lap joints we manufactured in the same method using the same materials with only the contamination varied.

2.3. Assessment of simulated kissing defects

Five of each of silicon grease, and Frekote contaminated lap joints along with five defect free mechanical control joints were tested to failure using an Instron 8802 servo-hydraulic test machine. The failure loads and shear strengths of the control joints and those containing defects are presented in Table 1. As expected the addition of the silicon and Frekote contaminations significantly reduce the failure load and shear strength of the joints by about 50%. Both contaminants have reduced the adhesion and hence the failure loads of the joints by approximately the same amount. Generally a reduction of adhesion area of about 11% resulted in a reduction of failure load by about 50%. A kissing bond is defined to give a reduction in shear strength of the bond by 80% [2] when the defect is over the entire bond. As the silicon grease and Frekote contaminations produced defects in a small patch in the bonded region rather than across the entire bond, it is considered that a reduction in joint strength of 50% for this type of defective joint indicates kissing defects. Failed samples of the mechanical control (defect free), thermal control (PTFE) and simulated defects (silicon grease and Frekote) were also inspected, see Fig. 3. The post mortem observations show that that there is a change in the failure modes between the joints without a defect and those with simulated defects. The uncontaminated bond failed via cohesive failure, which demonstrates good adhesion between the adhesive and adherend, however the contaminated bonds fail via adhesive failure. It has been suggested that the mode of failure of a bond caused by a kissing defect should be adhesive [2], which is confirmed as the mode of failure for the contaminated joints tested. A second observation is that the introduction of the Frekote and the silicon grease had visibly different effects on the adhesive. The silicon grease prevented adhesion between the adherend and adhesive in the area where it was applied on one adherend only; the adhesive remained bonded to the other adherend as shown in Fig. 3. The Frekote appears to have affected the adhesive and prevented adhesion of the adhesive on both adherends. Both contaminants were only introduced on one adherend, so the Frekote has penetrated through the thickness of the adhesive. The action of the Frekote has effectively removed the adhesive from the vicinity of the bond. As the definition of a kissing defect is the adhesive remains in the area of application but does not bond to the adherend, the Frekote has produced a defect that cannot be defined as a kissing defect. Furthermore, as Frekote has very low viscosity there was some bleeding from the area where the Frekote was applied, which led to it spreading into a larger area of the bond than was intended. In view of the two above reasons, i.e. the penetration of the Frekote into the adhesive and its low viscosity, it was concluded that Frekote was not suitable for introducing a controlled simulated kissing defect. Therefore the kissing defects in the current work are all simulated using silicon grease, as described in Section 2.2.

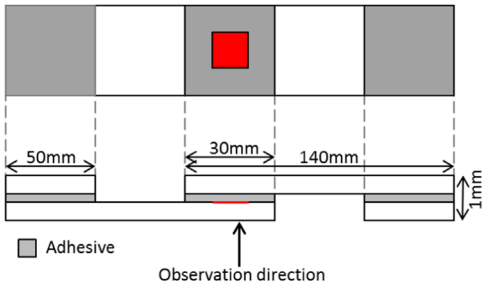

Fig. 2. Schematic of CFRP lap joint including contamination location.

Table 1
Failure load and effective adhesive area for failed lap joints containing no defect, Frekote and silicon grease.

Contamination	Failure load (kN)	Shear strength (kN/m^2)	Adhesive area (mm^2)
Control (no defect)	11.9 ± 0.4	13222 ± 444	900
Silicon grease	6.6 ± 0.5	7333 ± 625	800
Frekote mould release	6.0 ± 0.6	6666 ± 750	< 800

The PTFE insert samples were also inspected as a thermal control sample for defect identification. Ultrasonic c-scans have been taken of the PTFE and silicon defects using a 25 MHz very high frequency transducer, see Fig. 4. Generally ultrasonic inspection of composites uses transducer frequencies below 5 MHz [20] due to high levels of attenuation. As a higher frequency can resolve a thinner feature, the standard frequencies used for c-scanning composites are not able to resolve kissing defects. In the current case it has been possible to use very high frequency transducers able to resolve the thin defects of interest, which were

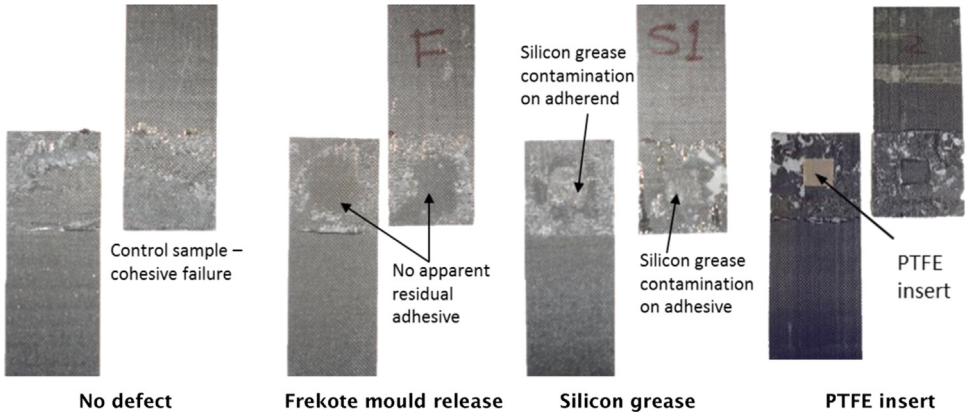

Fig. 3. Photos of adherends after failure showing variation of failure modes of the bond for an uncontaminated joint, a Frekote contaminated joint, silicon grease contaminated and PTFE insert joint.

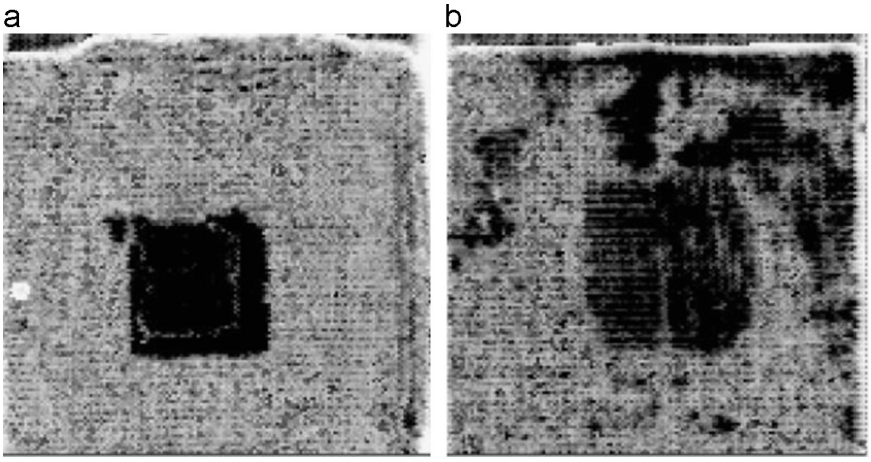

Fig. 4. Ultrasonic c-scans of (a) PTFE and (b) silicon lap joints using 25 MHz transducer, step size 0.2 mm.

not resolvable even with a 15 MHz probe. Fig. 4 shows both the PTFE and silicon grease contamination are clearly identified using the 25 MHz transducer. It could be claimed that the defects are not true kissing defects as they are detectable by very high frequency ultrasound, however as these defects are not detectable using standard ultrasound they can be commonly categorised as kissing defects. The purpose of these ultrasound images was to establish that the defects are not detectable using standard frequency ultrasound and to enable the location and extent of the contaminations to be established. There is an anomaly identified in the upper edge of the silicon grease lap which could be improper adhesion or could be delamination of the adherend introduced during the cutting of the adherends.

The results from the tests to failure of the silicon grease contaminated laps were used to define the loading parameters for the NDE. TSA tests were carried out at 3 ± 1 kN and the TSA mean load of 3 kN was also used as the static load for PPT. The aim of the tensile load was to create a bending moment in the sample that was sufficient to open the defects. Defects are found on the neutral axis of bending for the sample, as is typical for lap joint configurations; therefore, a relatively large tensile load at 50% of the failure load was selected for the tests to give the best chance of defect detection.

2.4. Experimental procedure

The IR detector used for both the TSA and the PPT was a Cedip Silver 480 M photon detector with an indium antimonide (InSb) sensor array with a detectable wavelength range of 2–5.5 μm. The detector is cooled using a Stirling pump maintaining an operating temperature of 77 K. The detector recorded at 383 Hz at the full detector array size of 256×320. The heating source used was a Nikon Speedlight SB-600, which is an external camera flash unit that was triggered remotely to provide surface heating to the bonded areas. The standoff distance between IR detector and specimen was 250 mm and the distance between flash and specimen was 150 mm.

The loading sequence was as follows. Each sample was clamped in the test machine and PPT was carried out on the unloaded samples. A load was applied to the sample up to the TSA mean load of 3 kN. PPT was carried out again at this load. The cyclic load of 3 ± 1 kN at 5 Hz was then applied and TSA was carried out. Once the TSA measurement was complete the sample was held at 3 kN and a repeat of the PPT was carried out. Finally the sample was unloaded and a final PPT test was carried out. Comparison of the unloaded PPT before and after loading was made to check for any clear signs of damage caused by the loading. Also, comparison of the loaded PPT before and after the cyclic loading was made to ensure that damage had not evolved.

3. Results

3.1. PTFE

Fig. 5 shows a sample of the TSA and PPT results for the PTFE inserts. TSA ΔT and phase data ($\Delta\phi$) are presented allowing analysis of any changes in the surface stress field and any phase shift obtained between the cyclic loading and the thermal response. Variation in TSA phase data shows areas where a range of factors may be affecting the response including non-adiabatic conditions, localised plasticity or localised heating. The TSA ΔT data shows a gradient from a lower value at the top of the bond (i.e. the free edge) to a higher value in the adherend at the lower edge of the bond, a typical contour plot is shown in Fig. 5a. The lap joint geometry results in an offset loading in each adherend which develops the stress gradient across the lap. This bending causes peel stresses in the lap and results in compression across the bond, as the bond is loaded in tension this compression reduced the tensile stress across the bond, causing the gradient, however the resultant stress remains tensile. It is notable that the PTFE insert is not visible in the TSA data indicating that its presence has no effect on the stress field. The TSA $\Delta\phi$ in Fig. 5b shows a uniform phase distribution across the PTFE insert. However at the upper and lower edges of the lap where the peel stresses are the largest there is a change in $\Delta\phi$, indicating some possible damage in the bond.

The PPT $\Delta\phi$ in Fig. 5c identifies clearly the PTFE insert prior to the application of load. The results of the PPT taken with the sample at a load of 3 kN also revealed the PTFE insert, see Fig. 5d. A comparison of profile plots across the width of the defects for the loaded and unloaded condition is shown in Fig. 6. The magnitude of $\Delta\phi$ between the surrounding well bonded area and the bonded area containing the PTFE was not changed by the addition of load. Therefore it can be concluded that the simulated PTFE defect is not being opened under this load thus the heat transfer path through the defect region is not altered. The PTFE is identified due to the contrast of thermal properties compared to the surrounding materials equally for both cases. The lack of change in $\Delta\phi$ suggests that it is not appropriate to use this kind of insert to represent a debond in an adhesive joint.

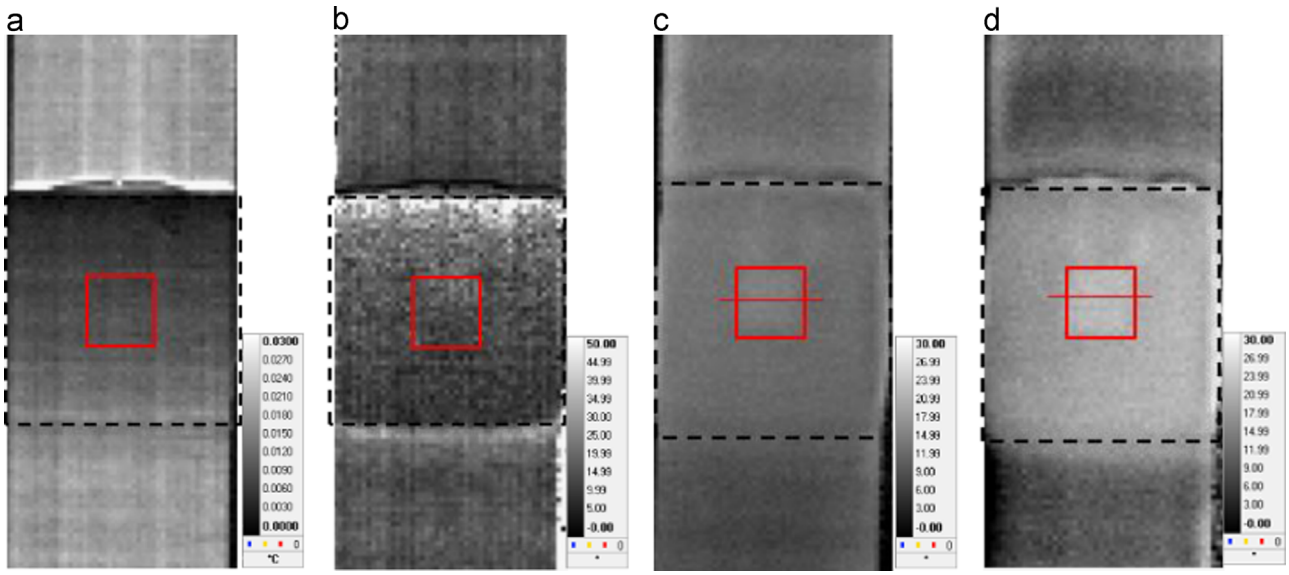

Fig. 5. PTFE insert results (a) TSA ΔT (3+1:kN), (b) TSA $\Delta\phi$, (c) PPT $\Delta\phi$ (0 kN) and (d) PPT $\Delta\phi$ (3 kN). Bonded regions are highlighted with a dashed box, defect locations with a solid red box and phase profile data used in Fig.6 taken across defects with a line.

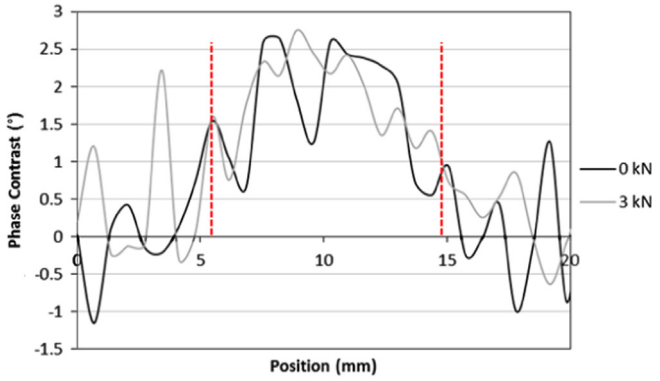

Fig. 6. PPT phase contrast data taken along the profile line across the PTFE insert for both the unloaded and 3 kN static loaded PPT results. Vertical dashed lines mark the extent of the defect.

3.2. Silicon grease

Similarly to the PTFE insert lap joint, the silicon grease contaminated joint TSA ΔT data shows a gradient across the joint, see Fig. 7a. The TSA ΔT data is unable to identify any clear anomalies in the stress distribution through the joint with the silicon contamination; however, the TSA $\Delta\phi$ data shown in Fig. 7b does identify a discontinuity in the joint. The TSA $\Delta\phi$ data shows the greatest contrast at the edges of the lap joint where the largest peel stresses are found. It also shows variations in $\Delta\phi$ at the upper and lower edges of the defect. The TSA $\Delta\phi$ data suggests that the loading of the lap is opening the bond where the silicon grease was placed, which is then having an effect on the coupling of the thermomechanical behaviour at the upper and lower edges of the defect.

PPT is unable to identify the silicon grease when the joint is unloaded, see Fig. 7c, which implies that the contamination has little effect on the heat transfer through the defect region. This is the expected thermal response of a kissing defect. When the joint is loaded to 3 kN the data shown in Fig. 7d shows that a defect is identified at the upper edge of the lap possibly due to the peeling at this region. More importantly however, the silicon grease insert is clearly identified indicating that sufficient load has been applied to open a gap between the adhesive and adherend where the silicon grease is present. The detection of such a defect using PPT relies upon sufficient thermal contrast being introduced to cause a detectable variation in the PPT $\Delta\phi$ data. The profile plot data shown in Fig. 8, taken horizontally through the central region of the defect, see Fig. 7c and d, shows that the phase contrast is greatly increased when the joint is under load thus demonstrating promise that the addition of load may enable wider defect detection using PPT.

4. Thermal finite element modelling

The discussion from the previous section postulated that a kissing defect is detectable when sufficient load is applied to open the defect and create a gap. To further explore this idea a finite element model (FEM) of PT and PPT was created to identify the minimum detectable gap using the current experimental set up. The heat transfer model used here was developed in [21] so the details are not provided in the present paper. The model does not include the addition of load but simulates the opening of the defect by increasing the defect thickness. The defect material is taken as air and, the thickness of the defect is varied between 50 and 200 μm.

Fig. 9a shows the surface thermal contrast (T_c) between the defect and defect-free regions plotted against time. Fig. 9b shows that the maximum value of T_c increases with increasing defect thickness as the heat paths through defect and non-defect regions are increasingly varied. Using the detector sensitivity as a detectability threshold, shown as the dashed horizontal line at 20 mK in Fig. 9a and b, a minimum thickness of an identifiable gap of approximately 75 μm is required for the 10 mm wide defect in the CFRP lap joint to be detected above the threshold. This means that gaps below 75 μm are undetectable. The temporal duration of T_c remaining above this threshold is also proportional to the thickness of the air gap making the detection of thinner defects also dependent on suitable recording frequency for the detector. Although not considered here, the lateral extent of an air gap will also influence the T_c obtained as this will further alter the relative heat path through the component.

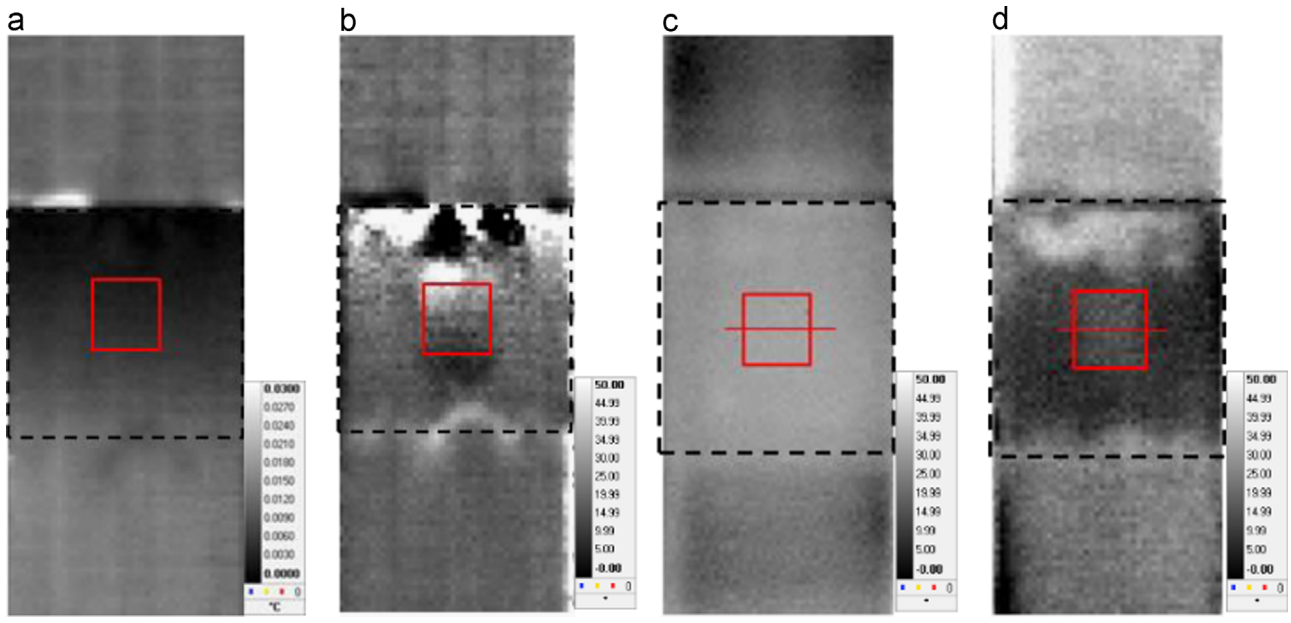

Fig. 7. Silicon grease contamination results (a) TSA ΔT (3 ± 1kN), (b) TSA $\Delta\phi$, (c) PPT $\Delta\phi$ (0 kN) and (d) PPT $\Delta\phi$ (3 kN). Bonded regions are highlighted with a dashed box, the defect locations with a solid red box and phase profile data used in Fig.8 taken across defects with a line.

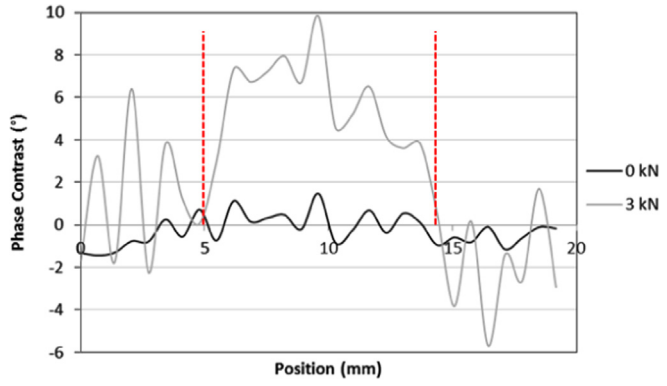

Fig. 8. PPT phase contrast data taken along the profile line across the silicon grease contamination for both the unloaded and 3 kN static loaded PPT results. Vertical dashed lines show the extent of the defect.

5. Application in an industrial setting

5.1. Equipment concept

The FEM results in the previous section highlight that only a small opening is required for a defect to be detected. Therefore it may be possible to use a loading device other than a test machine to open the defects that can be used for in-situ or on site studies. The concept of the application of a vacuum load to open a previously undetectable defect to enable defect detection is shown in Fig. 10 using vacuum position 1. Here the detector and the heat source are inside the vacuum chamber, with the camera control system outside the chamber. When the vacuum is applied the defect opens, the heat source is pulsed and the detector is triggered to capture the images for the PPT. Tightness tests using a vacuum on one site of the bond and monitoring any change in pressure are a common method of inspecting for leakage paths in adhesive bonds, thus that application of a vacuum to a bond is already available in industry.

The photon detector used in the work requires cooling to cryogenic temperatures which with modern systems is typically achieved using a Stirling cooling engine. There is some concern about applying a vacuum to such a device, but more importantly the cost of photon detector systems is high. Therefore a preliminary study has been undertaken using a low cost micro bolometer to investigate the feasibility of using such a device for thermographic NDE. Bolometers are relatively low cost and do not require cooling. However they are much less sensitive and operate at lower framing rates. The combination of a lower cost IR detector and the addition of load through a portable device would enable a practical NDE tool for in-situ inspection to be developed.

5.2. Test specimens

Initial studies testing the concept of the addition of vacuum load were undertaken by applying the vacuum load to the rear of the sample while PPT inspection was carried out from the other side, shown in Fig. 10 as vacuum position 2.

Trials were carried out using two test pieces. The first test piece comprised a 0.125 mm thick piece of aluminium adhered to a 0.5 mm thick CFRP panel, see Fig. 11a. The Araldite epoxy adhesive used in the lap joints has been used for this CFRP/aluminium bond. The total bonded area is 200x82 mm^2. A second test piece representative of an industrial application found in liquefied natural gas (LNG) carriers was also produced to demonstrate the concept may be applied to different material systems. The second piece consists of layered Triplex^{TM} material adhered to a CFRP plate. The Triplex comprises a 0.6 mm thick piece of aluminium with a layer of glass cloth adhered to both sides. Within the LNG carrier the Triplex is adhered to thick insulation blocks thus a stiffness mismatch is present between the two adherends of the bond. The stiffness mismatch has been recreated for laboratory testing using a CFRP plate as the second adherend. The adhesive used Araldite adhesive is also used for this test piece creating a total bond thickness of 1.4 mm. A 20 mm square silicon defect is introduced to the CFRP side of the bond with total bond dimensions of 250x150 mm^2, see Fig. 11b. It is noted that there was no noticeable distortion of the panels during manufacture.

5.3. Structural finite element modelling

A structural FEM was developed using Ansys 14.0 to investigate the amount of displacement likely to occur for the flexible

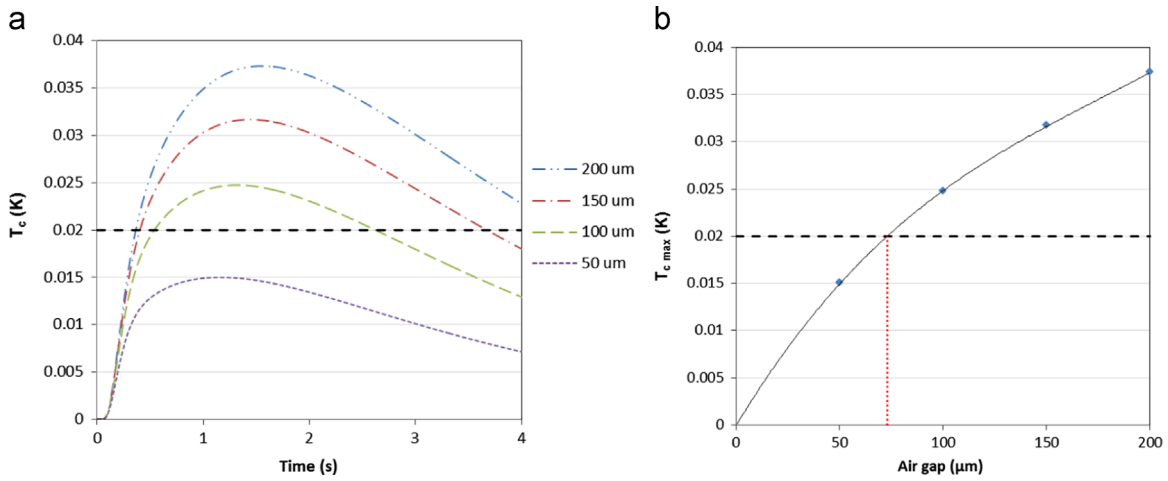

Fig. 9. (a) Thermal contrast through time between the surface temperature over the defect centre and a non-defect region for air gaps of 50–200 μm, (b) maximum thermal contrast produced for varied air gap defects.

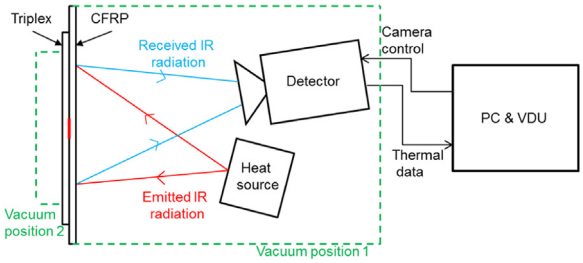

Fig. 10. PPT set up with vacuum load applied to the front of the sample (vacuum position 1) and the rear of the sample (vacuum position 2) while inspection is carried out on the front surface.

adherend under vacuum loading. The model assumed no adhesion at the kissing defect location. The edges of the defect were given a boundary condition of zero displacement, i.e. no propagation of the defect was allowed. The vacuum pressure applied to the aluminium was varied between 0 and 100% vacuum and the displacement was recorded. The displacement is that of the flexible adherend and the adhesive, as the simulated kissing defects were introduced between the CFRP and the adhesive. In Fig. 12 maximum and mean displacements across the defect are presented. The maximum displacement provides the size of opening that occurs at the centre of the defect, thus only identifying the centre point of the defect, which may cause an underestimation of defect size. This could result in misclassification of the defect. By using the mean displacement a more accurate prediction of defect size and hence more accurate classification is possible. In industrial NDE acceptance criteria are generally based on lateral size thresholds, which will be dictated by the application of the component under inspection. Misclassification occurs when there is insufficient contrast created across the full extent of a defect.

Fig. 12a and b show the maximum and mean displacement of the aluminium between the central point of the defect and the fixed edge under the application of various levels of vacuum loading. The results of the FEA are symmetrical so the results for half the defect are shown in Fig. 12. These results confirm that for this thin aluminium sheet the defect is being opened under very little applied vacuum pressure thus enabling defect detection as thermal contrast is created. The magnitude of opening of the defect is found to be far larger than that required for defect identification as expected for such a flexible adherend thus indicating that the concept of vacuum application should reveal the simulated kissing defects. The results of the Triplex/CFRP bond, shown in Fig. 12c and d, demonstrate that a low level of vacuum loading enables the defect to open and thus creates thermal contrast to enable defect identification.

5.4. Loading concept verification

To validate the concept of vacuum loading the vacuum is applied to the rear of the sample while the bond in inspected on the opposite side, shown in Fig. 10. A circular aluminium vacuum chamber of 120 mm diameter was held in place on the aluminium/triplex side of the bonds using 'tacky tape' commonly employed in composite materials processing. The bond was inspected from the CFRP surface for both panels. The vacuum chamber was connected to a pump which allowed the pressure reduction on the sample to be incrementally changed. The vacuum pressure was varied between ambient pressure, i.e. 0% vacuum, and maximum vacuum possible, 100%, using a vacuum pump.

Fig. 13a and b shows the PPT phase results of the same region of the aluminium and CFRP sample with no load applied and 100% vacuum loading. Features of the aluminium bond are indicated in Fig. 13a. The darker circular ring visible in the images (indicated by the dashed line) is due to the presence of the aluminium vacuum chamber attached to the rear of the sample while the strip across the centre (indicated by the dotted line) is where the aluminium located. Lines of fibre and resin are visible in the images as the CFRP had a low fibre volume fraction of 37%, hence there is a visible heat transfer contrast between resin and fibre as the fibre is sparsely distributed in the resin. Without the addition of load the silicon grease contamination is not visible in the phase data, however with the addition of the vacuum it is clearly identified in the centre of the image. Line profiles of data were taken across the defect location as indicated in Fig. 13 (solid line), for each level of vacuum applied; these are provided in Fig. 14a. The phase contrast is shown to increase with increased percentage vacuum as the defect is opened further and the heat path changes. Fig. 14b shows the mean $\Delta\phi$ obtained over the defect for each level of vacuum. The uncertainty is taken as the standard deviation of the phase values taken over the defect. There is an increase in the phase contrast as the vacuum is increased from 0 % to 60 %, as the defect is opened. Above 60% vacuum the changes in contrast are insignificant. This indicates at 60% the defect is as open as its maximum amount, without inducing propagation. Upon unloading of the sample the defect closed again and became undetectable, hence

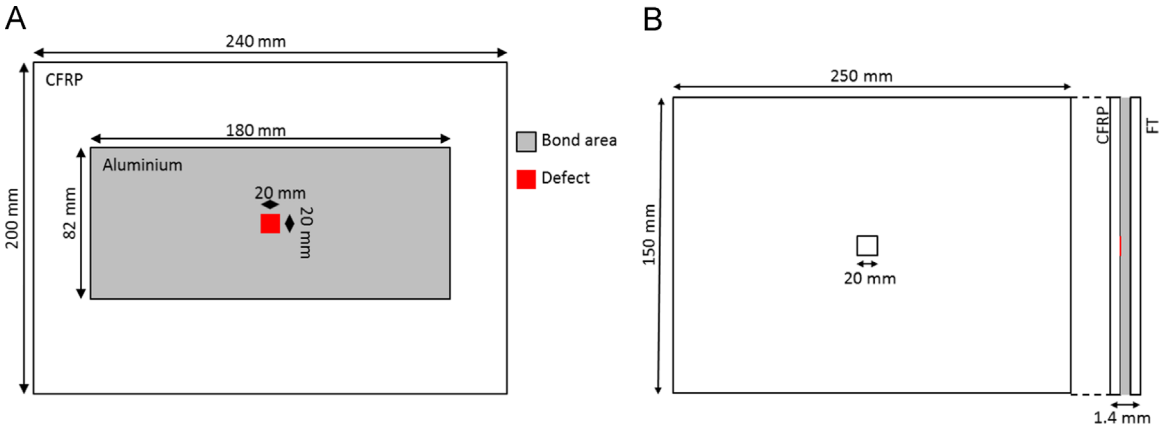

Fig. 11. Schematic of (a) CFRP – aluminium and (b) CFRP – Triplex bonded joints with silicon grease kissing defect for vacuum loading.

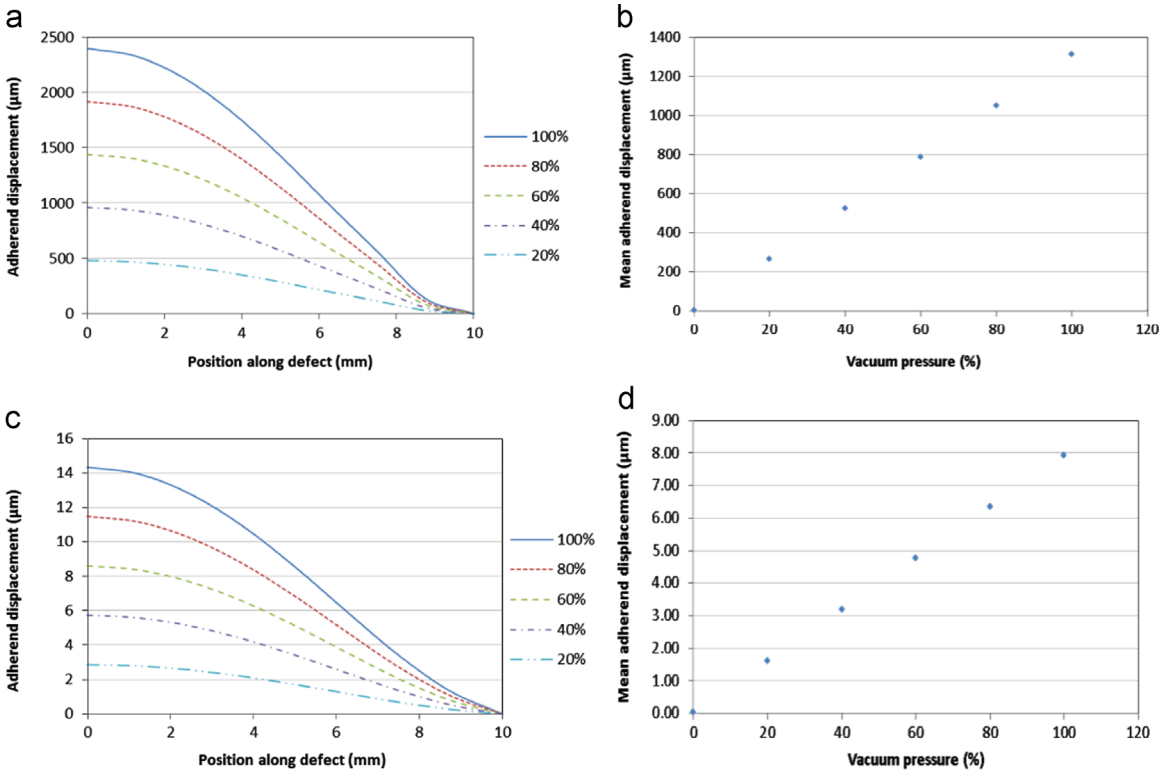

Fig. 12. FEA results of aluminium/CFRP bond showing (a) displacement across defect from defect centre (0 mm) to defect edge (10 mm), (b) mean adherend displacement for varied applied vacuum pressure and results from Triplex/CFRP bond showing (c) displacement across defect from defect centre (0 mm) to defect edge (10 mm), (d) mean adherend displacement for varied applied vacuum pressure.

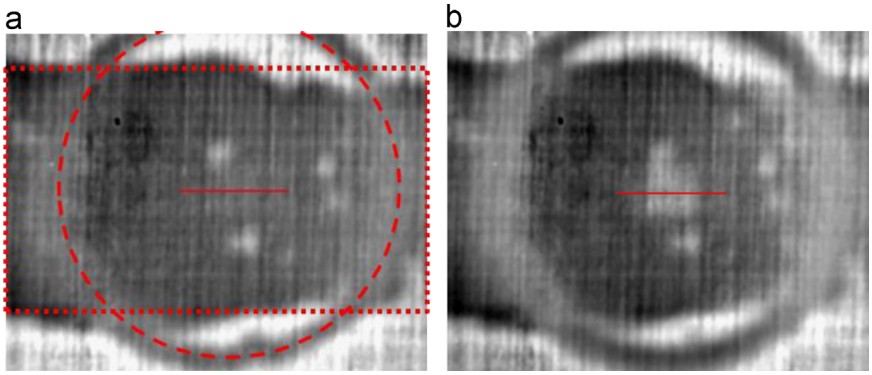

Fig. 13. PPT phase data for the CFRP/aluminium bonded sample (a) unloaded and (b) full vacuum applied to the rear of the sample. The vacuum chamber is highlighted by the dashed line and the aluminium bond is highlighted by the dotted line.

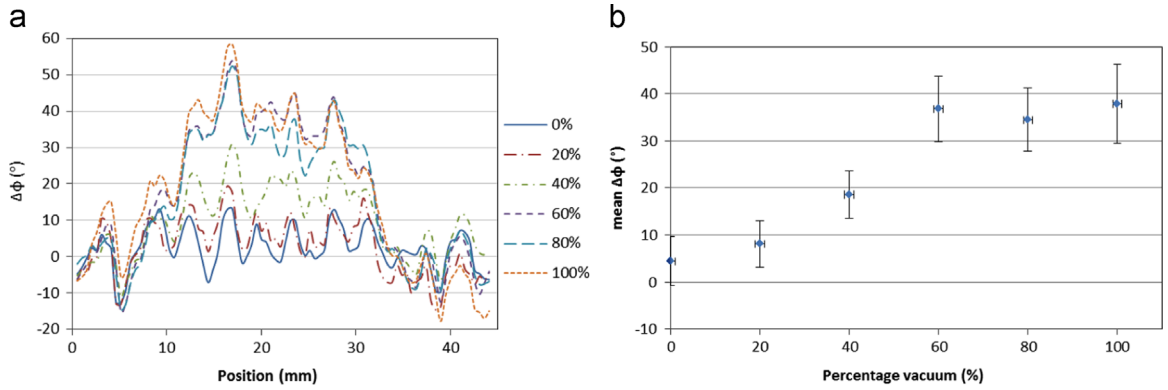

Fig. 14. (a) phase contrast profiles taken across the defect region under vacuum loading conditions of 100% vacuum and 0% vacuum and (b) the mean phase contrast between defect and non-defect regions taken across the width of the defect related to partial vacuum percentage applied.

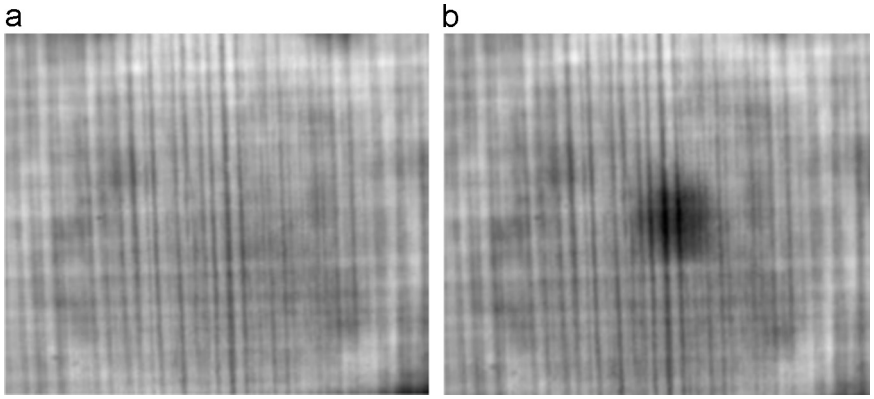

Fig. 15. PPT phase data for the CFRP/Triplex bonded sample (a) unloaded and (b) full vacuum applied to the rear of the sample.

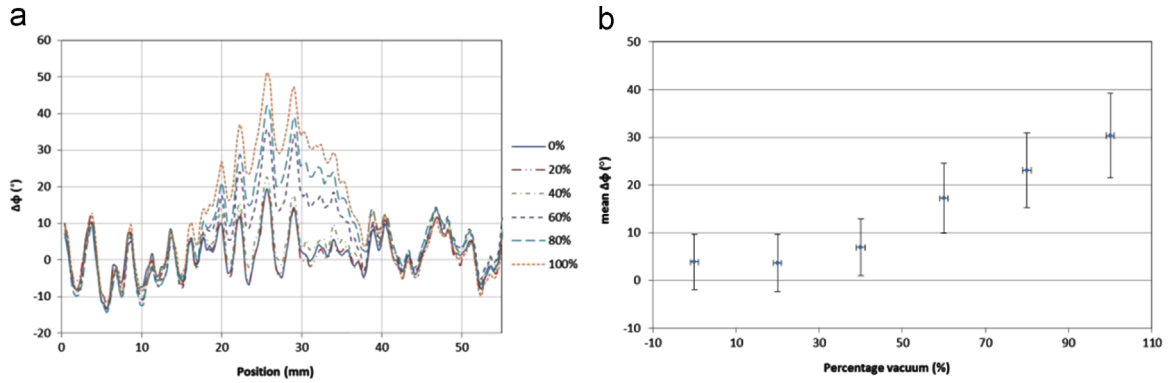

Fig. 16. (a) phase contrast profiles taken across the defect region under vacuum loading conditions of 100% vacuum and 0% vacuum and (b) the mean phase contrast between defect and non-defect regions taken across the width of the defect related to partial vacuum percentage applied.

showing that there was no plastic deformation. Further corroboration that the defect did not propagate is the close correlation of the bonded sections of the profile data as shown in Fig. 14a. As the defect did not propagate into 'well bonded' areas the loading remained non-destructive and hence the approach can be considered to be non-destructive. The amount of vacuum pressure required is dependent on the adherend material and the size of the defect to be identified. The defect becomes identifiable in the mean phase contrast data at just 40% of the maximum vacuum load in this trial.

Fig. 15a and b shows the PPT phase results of the Triplex/CFRP bond with no load applied and 100% vacuum loading. It is clear that without the addition of load the silicon grease contamination was not visible in the phase data; however with the addition of the vacuum it was easily identifiable in the centre of the image. The profile plot, in Fig. 16a, demonstrated that the regions away from the defect, i.e. the well bonded regions, were unaffected by the application of the vacuum, hence the defect was not propagated by the loading. An unloaded image was taken after the full vacuum was applied showing that permanent deformation had not been caused to the component by the vacuum loading. Fig. 16b shows the mean phase contrast between the defective and non-defective regions for each vacuum partial pressure applied. The defect becomes identifiable in the mean phase contrast data at just 60% of vacuum pressure.

A feasibility study was undertaken FLIR Tau 320 microbolometer was used to assess the use of a much lower specification detector than the current photon detector. The Tau 320 is an

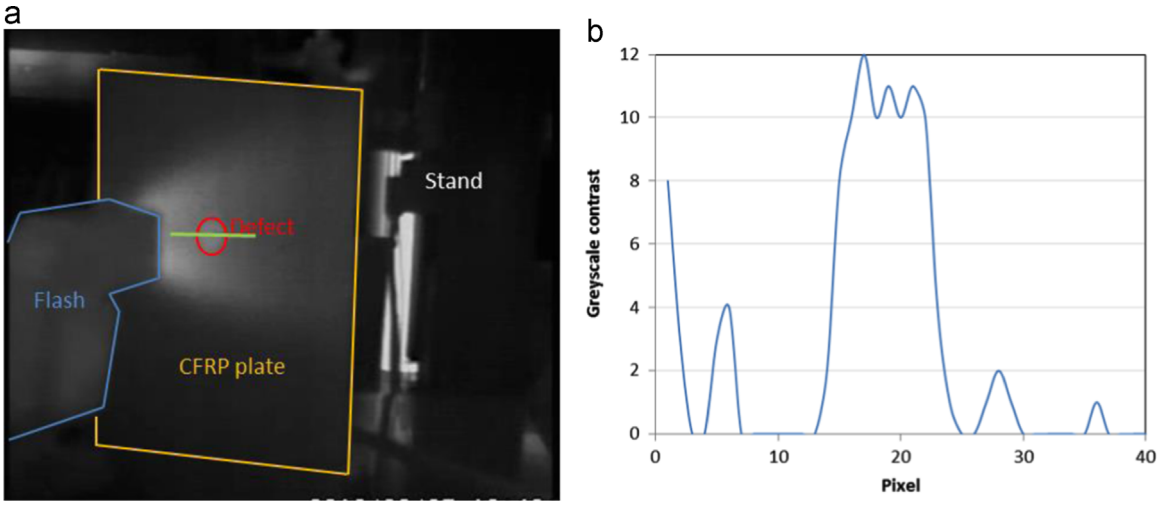

Fig. 17. (a) thermal data collected using bolometer and (b) greyscale profile data taken from solid green line in (a) across the defect site. (For interpretation of the references to color in this figure legend, the reader is referred to the web version of this article.)

uncooled system with a maximum frame rate of 25 Hz. A CFRP panel with PTFE defects to demonstrate that such a bolometer would be suitable for PT to identify shallow strongly contrasting defects. The fixed optics of the detector mean that the experimental set up is not ideal as highlighted in IR data in Fig. 17a, however, defect detection is still possible. The profile data taken across the identified defect is presented in Fig. 17b, which is given in greyscale as it is not possible to extract a calibrated video file. Bolometers are available that can collect data at higher frame rates and with increased thermal resolution that may be better suited for PPT.

6. Conclusions

Through the combined use of PPT and TSA it was found that the addition of a PTFE insert may not be classed as a defect. The addition of silicon grease to a bond provides a more realistic defect than the PTFE insert. The silicon grease contamination caused the bond to fail via adhesive failure, is not identifiable through material thermal contrasts and has caused a lack of adhesion in that region of the bond therefore there is confidence that a simulated kissing defect was produced. PPT cannot detect the simulated kissing defect unaided. When a load is applied to the specimen the defect is opened creating a gap that provides sufficient thermal contrast to enable PPT to identify the defect. A FE model identified how thick a gap must be to create enough thermal contrast to be detected. The modelled data predict that 10 mm wide air gaps with more than 75 μm thickness create sufficient thermal contrast for the current detector.

Vacuum loading has been successfully used to aid the identification of kissing defects. A feasibility study using a low cost bolometer for defect detection using PT was undertaken. These results demonstrate that through the use of portable vacuum loading and a lower cost IR detector a portable and financially viable means of inspection for industrial applications is possible. It should be noted that although the technique has been applied to adhesive bonded joints, the work is also relevant to inspection of debonds at the face sheet/core interface in sandwich structures as well as detecting defects in single skin composite components.

Acknowledgements

The Lloyd's Register Foundation, United Kingdom and the EPSRC, United Kingdom are acknowledged for their financial support of this work.

References

[1] Brotherhood CJ, Drinkwater BW, Guild FJ. The effect of compressive loading on the ultrasonic detectability of kissing bonds in adhesive joints. J Nondestruct Eval 2002;21:95–104.
[2] Marty PN, Desai N, Andersson J. NDT of kissing bond in aeronautical structures. In: Proceedings of 16th world conference on NDT, Montreal, Canada; 2004.
[3] Brotherhood CJ, Drinkwater BW, Dixon S. The detectability of kissing bonds in adhesive joints using ultrasonic techniques. Ultrasonics 2003;41:521–9.
[4] Yan D, Drinkwater BW, Neild SA. Experimental and theoretical characterisation of kissing bonds in adhesive joint using non-linear ultrasonic measurement. In: Proceedings of the AIP conference , Rhode Island, USA; 2010. p. 1190–89.
[5] Yan D, Drinkwater BW, Neild SA. Measurement of the ultrasonic nonlinearity of kissing bonds in adhesive joints. NDT&E Int. 2009;42:459–66.
[6] Ibarra-Castanedo C, Susa M, Klein M, Grenier M, Piau J-M, Ben Larby W, et al. Infrared thermography: principle and applications to aircraft materials. Furth, Germany: International Symposium on NDT in Aerospace; 2008.
[7] Rajic N. Principal component thermography for flaw contrast enhancement and flaw depth characterisation in composite structures. Compos Struct 2002;58:521–8.
[8] Genest M, Martinez M, Mrad N, Renaud G, Fahr A. Pulsed thermography for non-destructive evaluation and damage growth monitoring of bonded repairs. Compos Struct 2009;88:112–20.
[9] Tashan J, Al-mahaidi R. Investigation of the parameters that influence the accuracy of bond defect detection in CFRP bonded specimens using IR thermography. Compos Struct 2012;94:519–31.
[10] Maldague X, Marinetti S. Pulse phase infrared thermography. J Appl Phys 1996;79:2694–8.
[11] Shepard SM. Method and apparatus for detecting kissing unbond defects. United States Patent: US7083327; 2006.
[12] Dulieu-Barton JM, Stanley P. Development and applications of thermoelastic stress analysis. J. Strain Anal. 1998;33:93–104.
[13] Maldague X, Galmiche F, Ziadi A. Advances in pulsed phase thermography. Infrared Phys Technol 2002;43:175–81.
[14] Almond DP, Peng W. Thermal imaging of composites. J Mircosc 2001;201:163–70.
[15] Halmshaw R. Non-destructive testing. London: Edward Arnold; 1987.
[16] Ibarra-Castanedo C, Piau J-M, Guilbert S, Avdelidis NP, Genest M, Bendada A, et al. Comparative study of active thermography techniques for the non-destructive evaluation of honeycomb structures. Res Nondestruct Eval 2009;20:1–31.
[17] Junyan L, Qingju T, Xun L, Yang W. Research on the quantitative analysis of subsurface defects for non-destructive testing by lock-in thermography. NDT&E Int 2012;45:104–10.

[18] Marinetti S, Plotnikov YA, Winfree WP, Braggiotti A. Pulse phase thermography for defect detection and visualization. Proc SPIE: Thermosense XXV 1999;3586:230–8.
[19] Dulieu-Barton JM. Thermoelastic stress analysis. In: Rastogi P, Hack E, editors. Optical methods for solid mechanics: a full-field approach. Germany: Wiley-VCH Verlag GmbH & Co. KGaA; 2012.
[20] A. Kapadia, National composites network: best practice guide - non-destructive testing of composite materials; 2007.
[21] Waugh RC, Dulieu-Barton JM, Quinn S. Modelling and evaluation of pulsed and pulse phase thermography through application of composite and metallic case studies. NDT&E Int 2014;66:52–66.